
Article:
Dogan, H., Sims, N. orcid.org/0000-0002-6292-6736 and Wagg, D. (2023) Implementation of inerter-based dynamic vibration absorber for chatter suppression. Journal of Manufacturing Science and Engineering, 145 (8). 084502. ISSN 1087-1357

https://doi.org/10.1115/1.4062118

Implementation of inerter-based dynamic vibration absorber for chatter suppression

Hakan Dogan*

Department of Mechanical Engineering
University of Bath
Bath, BA2 7AY, United Kingdom
Email: hd805@bath.ac.uk

Neil D. Sims

Department of Mechanical Engineering
The University of Sheffield
Sheffield, S1 3JD, United Kingdom
Email: n.sims@sheffield.ac.uk

David J. Wagg

Department of Mechanical Engineering
The University of Sheffield
Sheffield, S1 3JD, United Kingdom
Email: david.wagg@sheffield.ac.uk

ABSTRACT

Chatter is one of the major issues that cause undesirable effects limiting machining productivity. Passive control devices, such as tuned mass dampers (TMDs), have been widely employed to increase machining stability by suppressing chatter. More recently, inerter-based devices have been developed for a wide variety of engineering vibration mitigation applications. However, no experimental study for the application of inerters to the machining stability problem has yet been conducted. This paper presents an implementation of an inerter-based dynamic vibration absorber (IDVA) to the problem of chatter stability, for the first time. For this, it employs the IDVA with a pivoted-bar inerter developed in [1] to mitigate the chatter effect under cutting forces in milling. Due to the nature of machining stability, the optimal design parameters for the IDVA are numerically obtained by considering the real part of the frequency response function (FRF) which enables the absolute stability limit in a single degree-of-freedom (SDOF) to be maximised for a milling operation. Chatter performance is experimentally validated through milling trials using the prototype IDVA and a flexible workpiece. The experimental results show that the IDVA provides more than 15% *improvement in the absolute stability limit compared to a classical TMD.*

*Address all correspondence for other issues to this author.

1 INTRODUCTION

It is well known that excessive vibrations due to chatter can lead to undesirable performance during machining, due to poor surface quality, low material removal rate, unacceptable accuracy, loud noise, and damage to the machine or tool. One approach to improve stability by suppressing chatter is to use passive control devices. Tuned mass dampers (TMDs), are inexpensive solutions that can be straightforward to implement, and have therefore often been used to mitigate chatter in machining operations. Hahn first employed a Lanchester damper, which consists of a damper with an auxiliary mass, to eliminate chatter in machining [2]. Tobias [3] proposed the use of vibration absorbers to mitigate chatter in machine tools. Subsequently, Rivin and Kang [4] presented a comprehensive study including a tooling structure design and development of a TMD to increase the stability of boring bars in cutting operations. Tarng et al. [5] utilised a piezoelectric inertia actuator working as a TMD for the elimination of the chatter in turning. They manually tuned the parameters by setting the natural frequency of the vibration absorber equal to the natural frequency of the cutting tool and achieved six times higher chatter stability.

In earlier studies, the parameters of vibration absorbers to suppress chatter were mostly chosen applying Den Hartog's method [6], or numerical / manual tuning strategies to obtain the optimal parameters. However, it is now well known that the machining stability is typically inversely proportional to the negative real value of the frequency response function (FRF) [7, 8]. Based on this relation, Sims [9] suggested a new analytical tuning strategy for vibration absorbers used to improve machining stability. Here, the fixed-points in the real part responses were utilised to derive analytical expressions for the optimal design parameters, following a similar approach to Den Hartog's method. Miguelez et al. [10] evaluated the chatter suppression in boring bars showing that Sims's method demonstrates a better performance than Den Hartog's method. They also presented a local analysis of the analytical expressions from Sims's method to obtain a better tuning frequency which improves the chatter suppression performance. Rubio et al. [11] studied the parameter optimisation for TMDs to increase chatter stability in a boring bar involving the structural damping. They showed the effectiveness of Sims's method over Den Hartog's method. As analytical expressions in Sims' method were derived for undamped structures, they also employed a numerical optimisation method to maximise the critical depth of cut and achieved a better performance than Sims's method.

The TMD concept has recently been investigated as a method to suppress vibrations and, more importantly, chatter in a variety of machining operations. Rashid and Nicolescu [12] employed a tunable damper mounted on a workpiece following the TMD concept to mitigate vibrations in milling. They used a viscoelastic spring to realise the stiffness and damping connection in parallel. Experimental results indicated reduced vibrations with the parameters tuned for the magnitude of the frequency response. However, the real part responses were not considered in tuning the parameters. Munoa et al. [13] developed a TMD with variable stiffness and damping for fixtures of a large workpiece. They used a rotary circular spring whose stiffness can be adjusted by rotation using a small electric motor, and eddy currents for the damping treatment of the TMD. An iterative tuning algorithm, where the optimal frequency is determined for each spindle, was applied. The effectiveness of the proposed damper was experimentally demonstrated with milling trials. Yang et al. [14] proposed a passive damper whose stiffness is adjustable by changing the rotational orientation of the mass block inside the damper. The device was effective against the variation in dynamic properties of the thin-walled workpiece due to the material removal. Yuan et al. [15] proposed another type of passive damper, where its stiffness can be adjusted by changing the length between the connections of a thin plate carrying a mass block. Similarly, Yuan et al.

[16] developed a TMD for a milling operation of the free-end of flexible cylindrical parts whose frequency can be set from the location of the sleeves fixed to a thin walled tube and the workpiece. Furthermore, applications of TMDs embedded in a boring bar and a milling tool have also been proposed in [17, 18]. Yadav et al. [17] embedded an absorber into a boring bar and experimentally showed the stability improvement. Ma et al. [18] developed a TMD integrated inside a rotating milling tool. The stability improvement of the proposed tool was only predicted by applying impact tests, but no cutting experiments were presented.

Traditional TMDs can suffer from limited vibration suppression performance, unless they employ high mass ratios. Therefore, enhancement of chatter performance of TMDs has been sought by investigating multiple, nonlinear and two-DOF TMDs. Yang et al. [19] showed that multiple TMDs outperformed a single TMD in chatter suppression performance for the same equivalent mass ratio. Nakano et al. [20] also employed multiple TMDs in end milling through a collect chuck, and experimentally verified chatter stability improvement. However, performance was only compared with an uncontrolled structure rather than a single TMD. Wang et al. [21, 22] examined a nonlinear TMD consisting of a friction-spring element in parallel connection to a linear spring and a linear viscous damper. Compared to the uncontrolled structure, the nonlinear TMD almost doubled the stability limit for a small mass ratio. Habib et al. [23] studied the effect of a cubic stiffness in parallel connection to a spring-damper arrangement. They concluded that a nonlinear TMD with a cubic stiffness can increase the robustness of the system against subcritical bifurcations for known operational spindle speeds. Further chatter stability improvement also succeeded with a two-DOF TMD. Yang et al. designed and implemented two-DOF TMDs applying two different damping mechanisms: friction plates [24] and eddy current dampers [25]. Even though they analysed chatter suppression by numerically tuning parameters for H_∞ optimisation in [24]; they did not specifically considered chatter stability in their work [25].

One of the most exciting recent developments in the passive vibration control community is the inerter, which was introduced by Smith [26] in 2002. The inerter is a relatively new mechanical device that generates forces proportional to the relative acceleration between its two terminals. This is in contrast to an idealised mass element, where the inertial forces are proportional to its absolute acceleration. There have been different types of inerter realisation proposed including rack-and-pinion inerters [26, 27], ball-screw inerters [28, 29], fluid-based inerters [30, 31], and small-scale inerters with living hinges [32, 1] (see also reviews in [33, 34]). Inerter-based vibration absorbers have been shown to improve dynamic performance in a wide range of engineering fields, including vehicle suspension systems [35, 36], aircraft landing gear [37, 38], and civil engineering applications [39, 40, 41, 42]. Among the many possible inerter-based layouts, three well-known layouts utilised in vibration suppression and isolation systems are the tuned inerter damper (TID) [39], the tuned mass damper inerter (TMDI) [43] and the tuned viscous mass damper (TVMD) [44]. These layouts have mostly been applied by deploying them between two different parts of the structure (e.g. between two storeys) or with a grounded connection. However, Hu and Chen [45] focused on inerter-based dynamic vibration absorbers (IDVAs), which are applied in a similar manner to classical TMDs, by replacing the damper in the TMD with an inerter-based layout. Their numerical evaluation investigated six different IDVA layouts, and showed improvements for both H_∞ and H_2 vibration absorption performance for all the layouts except where the layout consisted only of an inerter in series or parallel to the damper. The advantages of some of these layouts over a classical TMD were also reported for isolation performance in [46]. Analytical tuning methods for these IDVA layouts were studied by employing the fixed-point theory in [45, 46, 47].

The performance improvements obtained with an inerter in other applications makes them a

promising candidate for implementation in machining for chatter suppression. The potential benefits of inerters for machining stability were numerically examined in [48]. However, to the author's knowledge, such configurations have never been experimentally applied for chatter suppression in machining. The only previous work related to inerter application in machining is that of Wang et al. [49], who they examined the inerter to mitigate vibrations in milling. However, chatter suppression, which is a stability problem as distinct from forced vibration, was not considered. They also used a ball-screw inerter, which required a large space for implementation that may not be feasible in industrial applications. Furthermore, their inerter was clamped to the work table, which led to an additional grounded connection of the workpiece that may not be possible in practical fixturing scenarios. Physical realisation of an inerter-based configuration with the applicability of a traditional TMD could be a more preferable approach. This requires a smaller-scale inerter without a need for a ground connection. A pivoted-bar inerter device that meets these requirements was developed in a previous study [1]. However, it focused on the design study and its dynamic test was limited to the impact hammer test focused on vibration suppression. In this paper, such an IDVA is experimentally evaluated for chatter suppression in machining under cutting forces. The paper is organised as follows. Section 2 presents the regenerative chatter mechanism and the layouts of the IDVAs by deriving the equations of motions. Section 3 introduces the test scenario for the implementation in this paper. Then, the numerical optimisation for the tuning the parameters and numerical evaluations are discussed. Section 4 introduces the structural design of the IDVA and the experimental setup. The experimental results are discussed in Section 5. Section 6 discusses some interesting practical aspects of the IDVA approach. Finally, conclusions are drawn in Section 7.

2 THEORY

2.1 Regenerative chatter

Regenerative chatter can simply be explained through a milling system consisting of a rigid cutting tool and flexible workpiece as depicted in Fig. 1. Here, a single coordinate x is used for simplicity and consistency with the subsequent analysis. The rigid cutting tool causes waviness on the flexible workpiece's surface in each cut. Depending on the phase between wavinesses imprinted by consecutive cuts, the instantaneous chip thickness $h(t)$ could vary in a way that results in instability in the cutting operation, where vibrations and cutting forces exponentially grow. The regenerative mechanism was first explained by Tobias and Fishwick [7] and Tlusty and Polacek [8] for continuous cutting operation. For interrupted cutting, such as milling, the cutting force dynamically changes in direction and magnitude due to the rotating tool, which makes the stability analysis of the milling operation more complicated. In order to predict the milling stability, Budak and Altintas [50] proposed the zero-order approach where the directional milling force coefficients are averaged using a Fourier series expansion. This approach provides a fast and accurate stability prediction in milling operations for high-immersion cuts.

Assuming that the cutting force is proportional to the removal chip area and following the zero-order approach, the stability limit for an SDOF system (flexible in the x-direction) is predicted as [50, 51]:

$$a_{lim} = \frac{-1}{\left(\frac{N_t}{2\pi}\right) \alpha_{xx} K_t \Re\{G_x\left(i\omega_c\right)\}} \tag{1}$$

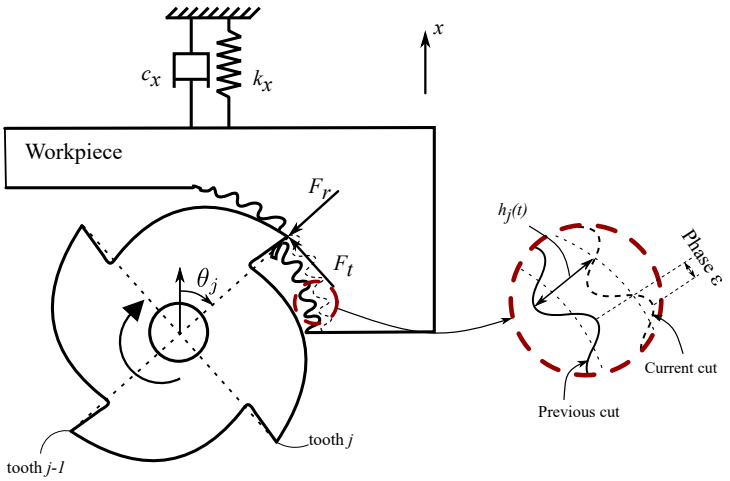

Fig. 1: Regenerative chatter mechanism in a milling system consisting of a rigid cutting tool and a flexible workpiece [50, 51].

where a_{lim} is the axial depth of cut at stability limit, N_t is the number of flutes, K_t is the tangential cutting stiffness, $G_x(i\omega_c)$ is the FRF of the most flexible part in milling system, and ω_c is the chatter frequency, and j is $\sqrt{-1}$. In addition, α_{xx} is the directional coefficient in the x-direction, which is defined by the cutting conditions and is equal to the averaged value in the Fourier series expansion. The spindle speed as a function of the chatter frequency is written as

$$n = 60\left(\frac{\omega_c}{2k\pi + \epsilon}\right) \tag{2}$$

where k is the integer number of oscillations between each tooth pass and ϵ is the phase of the oscillations.

Depending on the sign of the term α_{xx}, the most negative or positive real part of the FRF determines the absolute stability limit, below which the cutting operation is always stable for each spindle speed. This paper considers improvement in only the absolute stability for the cases where $\alpha_{xx} > 0$. Therefore, the most negative real part of the FRF will be improved to increase the absolute stability limit. However, the same approach can identically be applied for the cases where $\alpha_{xx} < 0$.

The zero-order approach is an accurate method for cuts with high immersions, not for cuts with low immersions [52]. Therefore, only cuts with high immersions (half immersion) will be performed in this study. This will provide suitable information in order to evaluate the IDVA under cutting forces.

2.2 Inerter-based dynamic vibration absorber

The force generated by an inerter is proportional to the relative acceleration between its two terminals. The inerter force is written as:

$$F = b(\ddot{x}_1 - \ddot{x}_2) \tag{3}$$

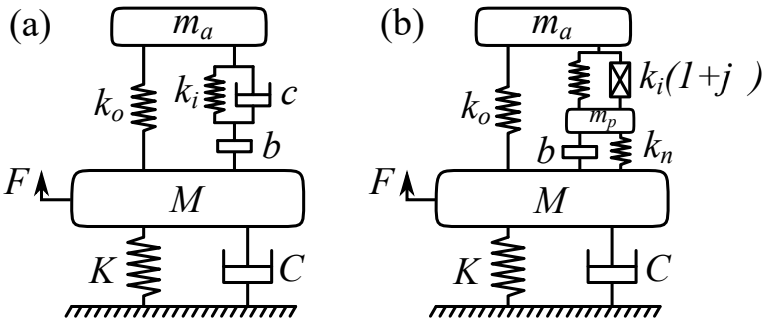

Fig. 2: Dynamic models of the IDVAs mounted on a SDOF main system: (a) the idealised IDVA and (b) the practical IDVA.

where b is the inertance with the units of kg and $(\ddot{x}_1 - \ddot{x}_2)$ is the relative acceleration between the inerter's terminals. An inerter-based dynamic vibration absorber (IDVA) can be obtained by replacing the damper in a TMD with an arrangement involving an inerter along with other structural elements such as springs and dampers. The new device arrangement is based on an inerter connected in series with spring and damper element, the so-called tuned inerter damper (TID).

If the milling system is dominated by one flexible mode far from the other vibration modes, the chatter occurs mostly due to the dominant vibration mode. For such cases, the milling system can be modelled as a SDOF system controlled by an IDVA under cutting forces as shown in Fig. 2. The milling system has parameters, mass M (kg), stiffness K (N/m), and viscous damping C (Ns/m). In comparison to Fig. 1, the $M-C-K$ system represents the dynamics of the flexible workpiece, and the forcing F arises due to the cutting forces F_r and F_t. Two IDVA layouts are considered to control the milling system and suppress chatter. The first one is the idealised IDVA as illustrated in Fig. 2(a). It has an auxiliary mass m (kg), an outer spring k_o (N/m), an inner spring k_i (N/m), an inerter b (kg), and a damper c (Ns/m) and is mounted on the milling system to suppress chatter vibration. However, the idealised IDVA layout for relatively small-scale applications (such as in milling operations) is difficult to physically realise. The mechanical model for the proposed IDVA in [1] – modified from the idealised layout due to practicality– is presented in Fig. 2(b).

The modified layout is adopted because even small parts in the structural design of IDVA (e.g. joint elements, small auxiliary components), especially for small inertance values, could act as a parasitic mass and detune the optimal design parameters. Therefore in Fig. 2(b), a parasitic mass m_p is added between the series-connected elements. Secondly, the more likely practical damping is considered and a complex stiffness $k_i(1+j\eta)$, where η is the loss factor, is employed. Finally, a spring element connected in parallel to the inerter is considered to model the notch stiffness k_n stemming from the inerter design as will be discussed in Section 4.

Here, the equations of motion of the SDOF system controlled with the practical IDVA, shown in Fig. 2(b), are derived in the Laplace domain as

$$\begin{aligned}
&Ms^2X_m + CsX_m + KX_m - bs^2\left(X_p - X_m\right) - k_n\left(X_p - X_m\right) - k_o\left(X_a - X_m\right) = F,\\
&m_ps^2X_p + bs^2\left(X_p - X_m\right) + k_n\left(X_p - X_m\right) - k_i\left(1+j\eta\right)\left(X_a - X_p\right) = 0,\\
&m_as^2X_a + k_o\left(X_a - X_m\right) + k_i\left(1+j\eta\right)\left(X_a - X_p\right) = 0.
\end{aligned} \tag{4}$$

Table 1: Dimensionless design parameters for IDVAs

$\mu = \frac{m_a}{M}$	$\beta = \frac{m_p}{m_a}$	$\delta = \frac{b}{m_a}$	$\zeta_m = \frac{C}{2\sqrt{KM}}$	$\Omega = \frac{\omega}{\omega_m}$
$\kappa = \frac{\omega_p}{\omega_m}$	$\gamma = \frac{\omega_a}{\omega_m}$	$\alpha = \frac{\omega_b}{\omega_a}$	$\zeta_a = \frac{c}{2\sqrt{k_o m_a}}$	

*where $\omega_p = \sqrt{k_n/m_p}$, $\omega_a = \sqrt{k_o/m_a}$, $\omega_m = \sqrt{K/M}$, and $\omega_b = \sqrt{k_i/b}$

where X_p refers to the displacement of the parasitic mass m_p.

Using the dimensionless parameters in Table 1 and substituting $s = j\omega$, the dimensionless equations of motion in the frequency domain are derived from Eq. 4. The dimensionless equations of motion for the practical IDVA are determined as

$$\begin{aligned}
&\left(\left(-1-\delta\mu\right)\Omega^2 + j2\zeta_m\Omega + 1 + \gamma^2\mu + \kappa^2\beta\mu\right) X_m\left(\Omega\right) + \left(\delta\mu\Omega^2 - \kappa^2\beta\mu\right) X_p\left(\Omega\right) - \left(\gamma^2\mu\right) X_a\left(\Omega\right) = \Delta\left(\Omega\right), \\
&\left(\delta\Omega^2 - \kappa^2\beta\right) X_m\left(\Omega\right) + \left(\left(-\delta-\beta\right)\Omega^2 + \alpha^2\gamma^2\delta\left(1+j\eta\right) + \kappa^2\beta\right) X_p\left(\Omega\right) - \left(\alpha^2\gamma^2\delta\left(1+j\eta\right)\right) X_a\left(\Omega\right) = 0, \\
&\left(-\gamma^2\right) X_m\left(\Omega\right) - \left(\alpha^2\gamma^2\delta\left(1+j\eta\right)\right) X_p\left(\Omega\right) + \left(-\Omega^2 + \gamma^2 + \alpha^2\gamma^2\delta\left(1+j\eta\right)\right) X_a\left(\Omega\right) = 0.
\end{aligned} \tag{5}$$

The dimensionless frequency response functions for the practical IDVAs can be written in a generic form:

$$\tilde{G} = \frac{X_m}{\Delta} = \frac{R_n + jI_n}{R_d + jI_d} \tag{6}$$

A full expression for Eq. 6 derived from Eq. 5 as well as the expression for the idealised IDVA are given in Appendix A.

3 DYNAMIC PROPERTIES AND OPTIMISATION

3.1 Dynamic properties

In the remainder of this contribution, a flexible workpiece with a dominant vibration mode in one direction was considered for the test scenario. To realise this, an aluminium workpiece supported by a compliant mechanism was designed, as will be shown in the milling setup in Section 4. The compliant mechanism provided a distant (in terms of frequency) and most flexible vibration mode compared to the other modes in the dominant direction, thus ensuring that stability could be validated focusing on a single stability lobe of the flexible workpiece. A prototype of the IDVA, as will be introduced in Section 4, will be attached to this structure to suppress chatter in Section 5. Therefore, the modal parameters are presented here since they are required for the optimal parameters. The dynamic properties of the uncontrolled structure (without the prototype) were identified via an impact test as: natural frequency $f_n = 118$ Hz, modal mass $M = 10.7$ kg, and structural damping $\zeta_m = 1.9\%$.

3.2 Optimisation and numerical evaluation

The objective for chatter suppression is to maximise the most negative real part of $\tilde{G}(\Omega)$, which gives the improvement in the absolute stability limit as indicated in Eq 1. Thus, the objective

Table 2: Optimal dimensionless design parameters obtained for TMD, the idealised IDVA, and the practical IDVA. All parameters are obtained for $\mu = 0.037$ and $\zeta = 1.9\%$.

	β	κ	γ	α	δ	ζ_a	η
TMD	–	–	1.0497	–	–	0.1178	–
IDVA$_{idealised}$	–	–	1.0924	0.9534	0.0846	0.0159	–
IDVA$_{practical}$ ($k_{notch} = 0$)	0.0657	–	1.1202	1.5862	0.0326	–	0.4557
IDVA$_{practical}$ ($k_{notch} = 9000$N/m)	0.0657	1.2602	1.1116	0.9997	0.0960	–	0.6087

problem can be defined as

$$max\big(min\left(\Re\{\tilde{G}\,(\Omega)\}\right)\big) \tag{7}$$

which is to be solved by optimising design parameters $[\gamma, \alpha, \delta, \zeta_a]$ and $[\gamma, \alpha, \delta, \eta]$ for the idealised and practical IDVAs, respectively. A range of possible numerical optimisation algorithms could be used; in the present study, the self-adaptive differential evolution (SaDE) algorithm [53, 54] was run in Matlab to numerically solve the objective problem.

The optimisation problems for both layouts were solved for mass ratio $\mu = 0.037$ and main damping ratio $\zeta_m = 1.9\%$. For the practical IDVA in Fig. 2(b), the parasitic mass and the notch stiffness were considered with the related dimensionless parameters $\beta = 0.0657$ and $\kappa = 1.2602$ for the same mass ratio and the main damping ratio. Furthermore, the case where there is no notch stiffness ($\kappa = 0$) in the practical IDVA was also considered. The dimensionless optimal design parameters are presented in Table 2 in comparison with the optimal design parameters for a classical TMD. The real part frequency responses obtained from the optimal design parameters are illustrated in Fig. 3. The IDVAs provided considerable improvement compared to a classical TMD by increasing the most negative real part responses by 20% for the idealised IDVA and 22% for the practical IDVA with $k_n = 9000$ N/m. The performances of the idealised and practical IDVAs with zero and non-zero notch stiffnesses were comparable.

4 THE IDVA AND EXPERIMENTAL SETUP

The prototype for the IDVA with a pivoted-bar design, which was developed in [1] (as shown in Fig. 4) was utilised to control the chatter suppression in milling operations. The stiffness caused by notch hinges utilised as the pivot points in the inerter (to avoid possible backlash and friction problems) was estimated as 9000 N/m. Complex stiffness is provided using a gel damper consisting of a mixture of two liquids which takes a gel form and remains in between two plates once they mix. The damping and stiffness properties of the gel is set with the mixing ratio of the liquids and dimensions of the gel [55, 56]. The gel plate with a mass of 26 gram in the gel acts as the parasitic mass. In order to identify the actual parameters, each component of the absorber was separately tested by fixing its base and applying an impact hammer for different masses added (to the top side of the outer spring, the gel plate for the gel damper, and the ends of the inerter bar for the

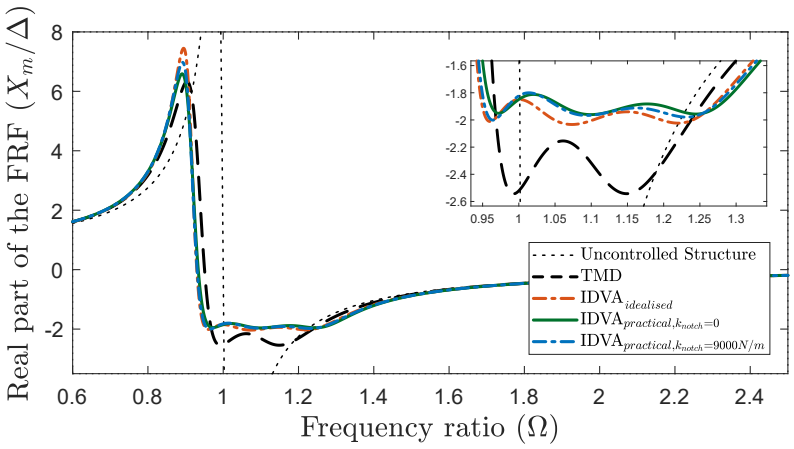

Fig. 3: Real part responses of the FRF of the uncontrolled structure, TMD, the idealised IDVA, and the practical IDVA (for zero and non-zero notch stiffnesses) using the optimal design parameters presented in Table 1.

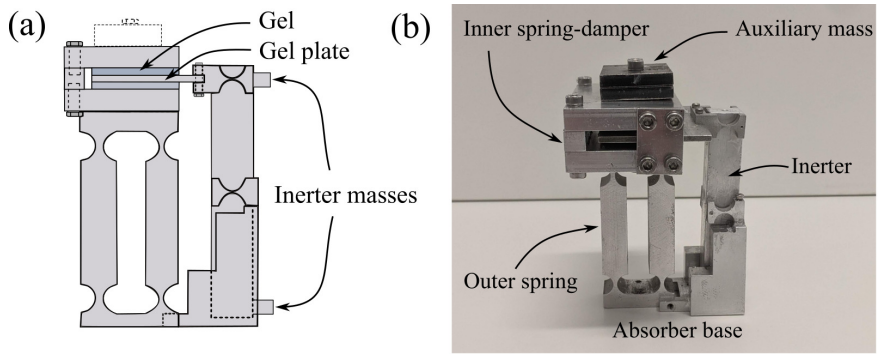

Fig. 4: (a) The schematic view of the complete absorber and (b) an image of the manufactured prototype [1].

inerter) [1]. The parameters were found to be $k_o = 251.89$ kN/m, $k_i = 24.97$ kN/m, $\eta = 0.522$, and $b = 0.0162$ kg for no adjustment mass.

The milling setup with the flexible workpiece is presented in Fig. 5, where the prototype is mounted on an Aluminium alloy (7075-T6) workpiece from the top surface. As mentioned in Section 3.1, the compliant mechanism provided a distant (in terms of frequency) and most flexible vibration mode compared to the other modes in the dominant direction. Consequently the dominant vibration occurs on in horizontal x coordinate as labelled on Fig. 5. An accelerometer (PCB 353B18) fixed to the workpiece in parallel to the flexible mode (x-direction) and an impact hammer (Dytran 5800B2) were used for the FRF measurement. The accelerometer PCB 353B18 was also utilised for the chatter detection in milling trials A proximity sensor attached to the spindle facing the tool holder was utilised to detect one revolution of the tool. The data streaming from the sensors was collected using an NI DAQ USB-4431 data acquisition system.

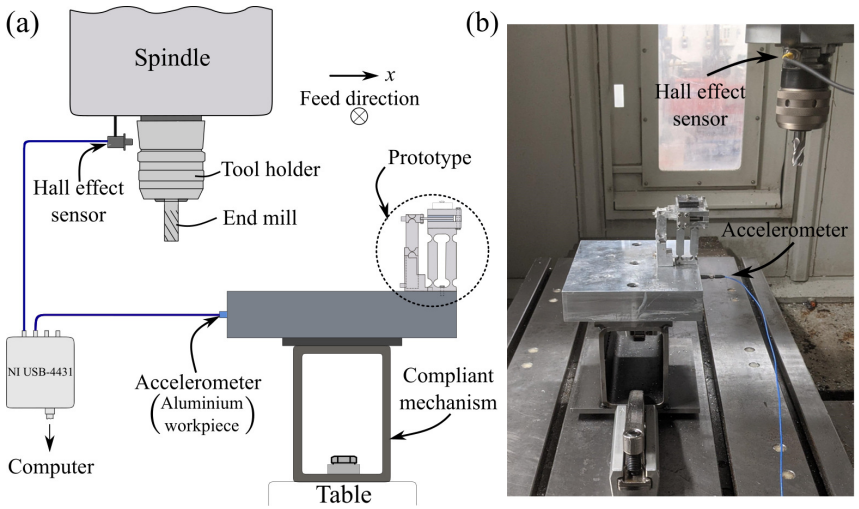

Fig. 5: (a) The illustration of the whole experimental setup and (b) an image of the setup in the CNC machine.

Table 3: Optimal dimensional design parameters of the practical IDVA (for $\mu = 0.037$, $\zeta_m = 1.9\%$, $m_p = 0.026$ kg and $k_n = 9000$ N/m), and the actual value for each element.

	k_o (kN/m)	k_t (kN/m)	η	b (kg)	$\Re(G)_{min}$ (m/N)
IDVA$_{optimal}$	268.93	25.80	0.6087	0.038	-3.33×10^{-7}
IDVA$_{actual}$	251.89	24.97	0.5217	0.038	-3.72×10^{-7}

5 EXPERIMENTAL VERIFICATION

Chatter stability performance was experimentally evaluated through milling tests for the workpiece using an end mill with a diameter of 16 mm, 4 flutes, and a constant 30° helix angle. Cutting coefficients were mechanistically identified as $K_t = 660$ N/mm^2 and $K_n = 180$ N/mm^2 in the tangential and radial directions, respectively. Down-milling operations with a half radial immersion (8 mm) and a feed of 0.04 mm per tooth were considered during the cutting operations. The prototype was set for $\mu = 0.037$. Considering the modal parameters of the workpiece-compliant system, dimensional optimal design parameters are presented in Table 3 with the actual parameters of the elements. The optimal parameters were obtained for $\beta = 0.0657$ and $\kappa = 1.2602$ (due to the parasitic mass of 0.026 kg and the notch stiffness of 9000 N/m).

Experimental real part FRF responses of the controlled structure are presented in Fig. 6 in comparison with the uncontrolled structure. For comparison purposes the numerical predictions for an idealised and optimally tuned TMD, and for an idealised and optimally tuned IDVA, are also shown. Numerically obtained results showed that the IDVA with actual design parameters attained an improvement by suppressing the most negative real part from -4.33×10^{-7} m/N in the case of TMD to -3.72×10^{-7} m/N, which implies a 14% percent improvement. The most negative real part in the modal test is close to the expected value in the numerical analysis for the practical IDVA with actual parameters. However, there is a deviation in the negative real part response between

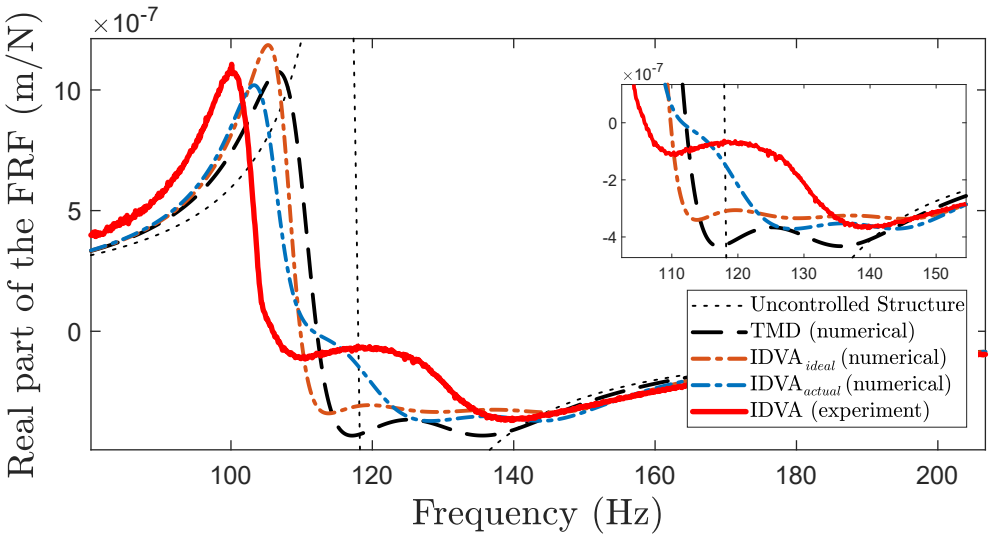

Fig. 6: The real part response obtained from the impact hammer test is in comparison with the real part responses of the uncontrolled structure, TMD and the practical IDVA with the optimal design parameters and actual parameters as given in Table 3.

110 Hz and 135 Hz. The reason for this could be the slight divergence in actual parameters of the components in the assembly from the values obtained from tests for individual elements.

Using these FRFs, the stability lobe diagrams (SLDs) for uncontrolled structure, TMD, the ideal IDVA, and the practical IDVA with actual design parameters and the prototype are predicted as demonstrated in Fig. 7. The SLD obtained from time domain simulations [57] is presented in the figure along with the SLD obtained using the zero-order approach. Both SLDs show a good match, except for the double period chatter observed above 4500 rpm. While the zero-order approach does not capture the double period chatter or flip bifurcations, it accurately represents the absolute stability limit, which is the main interest of this study. Therefore, the results are evaluated using the zero-order approach. The absolute stability limit in the SLD estimated from the experimental FRF was improved from 3.85 mm to 4.46 mm compared to the TMD result: a 16% improvement. Considering the uncontrolled structure, the 4.46 mm stability limit obtained by the prototype corresponds to more than a 4.5 fold increase in the stability. The stability predictions based upon the experimental data exhibit a wider stable region in between the lobes due to the deviation in the negative real part response between 110 Hz and 135 Hz. This is associated with the slight mis-tuning of the experimental device, and suggests that the IDVA could also be used for enhancement in stability pockets if parameters are tuned for this objective.

To experimentally confirm this chatter stability prediction, a series of milling experiments were conducted near the zeroth lobe for the uncontrolled and controlled structure, to validate the performance of the prototype. The occurrence of chatter was detected by once-per-revolution sampling in the time-domain, a Poincaré map, and appearance of chatter frequency in the frequency domain. Data points were sampled once per revolution; synchronised or low-variance samples indicate stable cuts whilst higher variances indicated the presence of chatter [58]. Also, only spindle and tooth passing frequencies (and their harmonics) are observed in the FFT spectrum in stable cuts. If chatter exists, the chatter frequency emerges in the frequency spectrum. Therefore, each

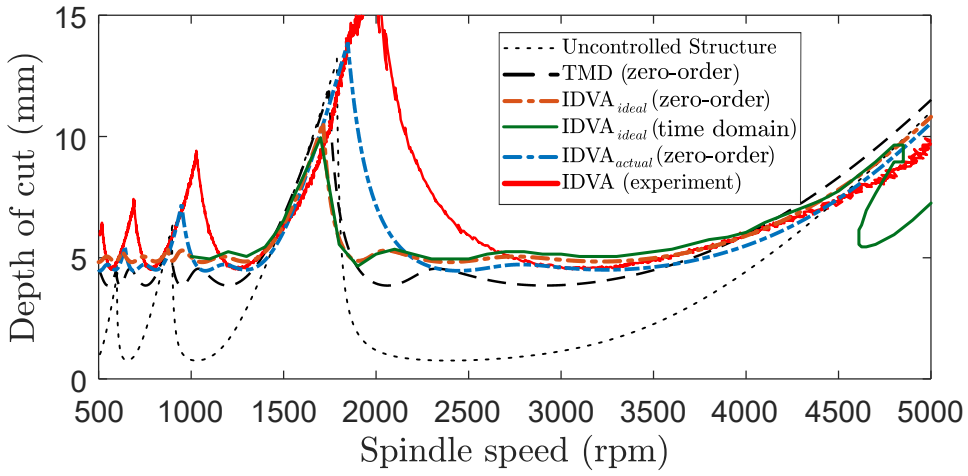

Fig. 7: Stability lobe diagrams obtained from the real part FRF responses (optimally tuned TMD and IDVA with actual parameters) in Fig. 6 including the time domain simulation for the ideal IDVA and experimental response

experimental test was assessed for stability using these three analysis techniques.

Cutting results are summarised in Fig. 8 with symbols indicating stable, marginal, or unstable cuts in the milling trials. The stability border was first experimentally validated for the spindle speed of 2800 rpm. For the uncontrolled case stable cuts were observed with a 0.8 mm depth of the cut (Point A) and the system became unstable for a depth of cut of 1.2 mm (Point B). For the controlled case, cutting tests the stability boundary was verified using depths of cut from 3 mm to 5 mm, with the instability beginning at 4.8 mm (Point E). In order to verify the stability pocket, additional cuts were performed for the lower and upper spindle speeds from 2400 rpm to 4200 rpm as shown in Fig. 8.

Fig. 9 shows more detailed analysis of the transition from stable cut to unstable cut, for the scenarios labelled A-E in Fig. 8. It can be seen from Fig. 9 that for Point A the once-per-revolution data points are synchronised, the Poincaré map exhibits a low variance, and the FFT spectrum is dominated by forced vibrations at the spindle and tooth passing frequencies. This indicates a stable scenario. In contrast, for Point B, the once-per-revolution samples become unsynchronised, the Poincaré map exhibits high variance, and the FFT is dominated by the chatter frequency that results from the unstable cut. In general, for the FFT spectra the spindle frequency is more dominant than the tooth passing frequency due to the existence of runout [59]. For the controlled case at the same spindle speed, a stable cut was achieved up to 4.4 mm depth of cut (Point C, 2800 rpm, 3 mm) and (Point D, 2800 rpm, 4.4 mm) as shown in Fig. 8. Chatter only occurred for the depth of cut of 4.8 mm (Point E, 2800 rpm, 4.8 mm)

To summarise, the milling trials have shown excellent agreement with the stability lobe predictions, substantial performance improvements compared to an uncontrolled system, and more effective performance than that predicted for a classical and idealised tuned mass damper.

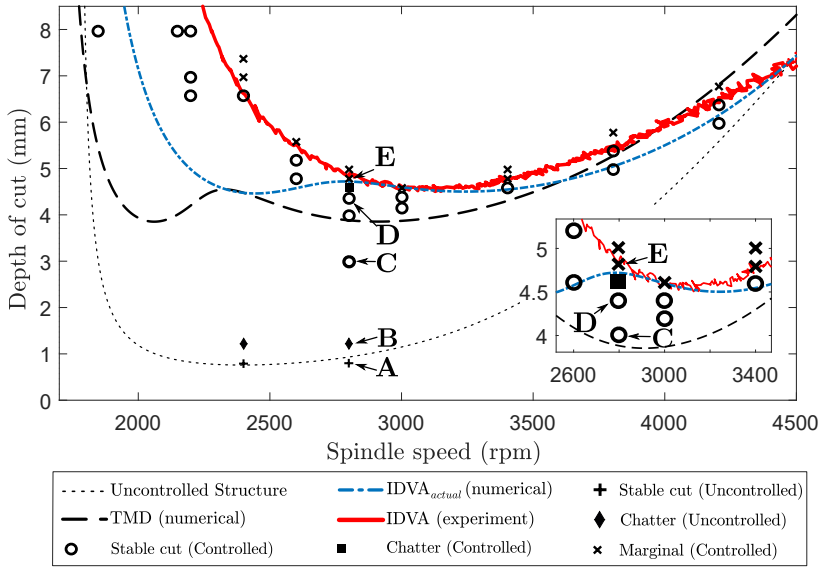

Fig. 8: Stability lobe diagrams with the simulated and experimental cuts.

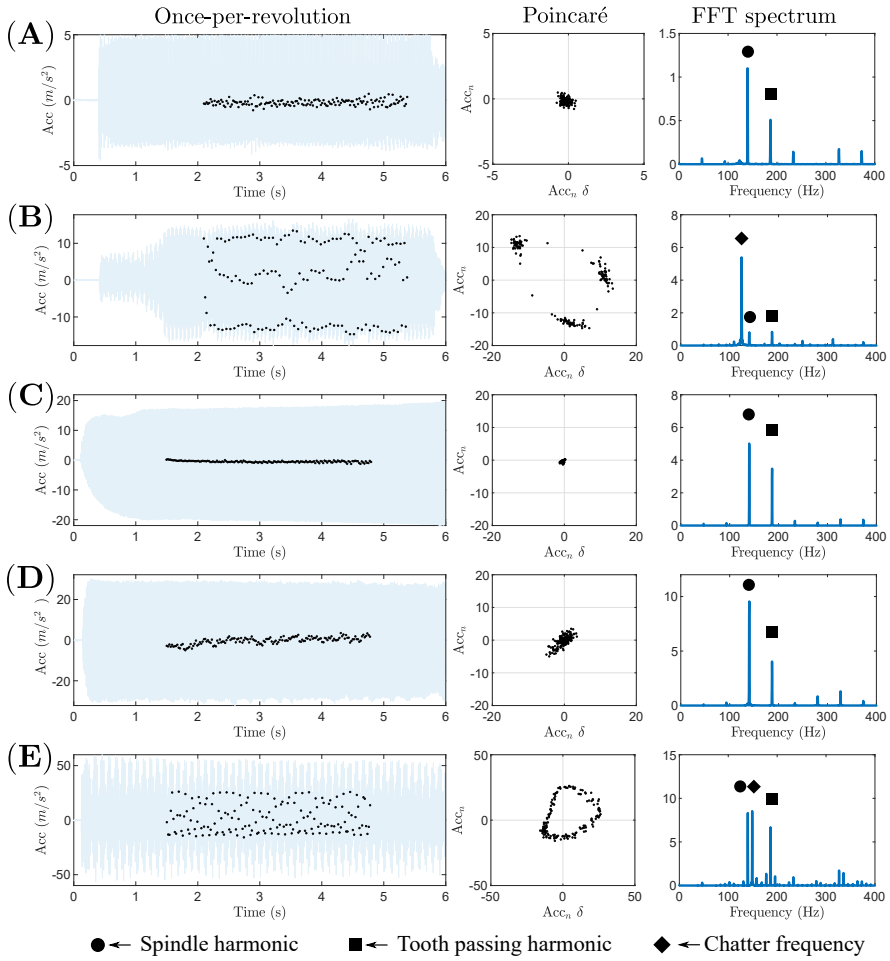

Fig. 9: Once per revolution samples, the Poincaré maps and the FFT spectrums showing different axial depth of cut for spindle speed of 2800 rpm for uncontrolled and controlled cases.Uncontrolled structure: stable cut A(2800 rpm, 0.8 mm) and stable cut B(2800 rpm, 1.2 mm), and controlled structure: stable cut C(2800 rpm, 3 mm), stable cut D(2800 rpm, 4.4 mm) and chatter E(2800 rpm, 4.8 mm).

Table 4: The mean and standard deviation values for the Monte Carlo simulation.

	K (kN/m)	f_n (Hz)	ζ_m
Mean	5881.8	118	0.019
Standard deviation (σ)	20%	1%	20%

6 DISCUSSION

Two aspects are worthy of further discussion: the practical design of the device, and its robustness to variations in the dynamics of the milling system.

In terms of practical design, it is acknowledged that the proposed design of the inerter-based absorber was primarily focused on proving its concept and as such, no particular attention was given to reducing the volume of the required damper. Although it is assumed that the inerter-based absorber would require a similar amount of space as a TMD does, it has the potential for volume reduction, given its superior performance in comparison with a TMD of the same dimensions. In this study, however, there is no significant reduction in volume compared to a TMD as the design was considered a proof of concept only. A volume reduction compared to the current version of the IDVA would be possible with further design work.

In terms of the robustness of the proposed design, it is acknowledged that the performance of any vibration absorber can be sensitive to the dynamic properties of the structure being controlled. For example, the initially identified dynamic parameters of the milling system can involve uncertainties due to the system identification process, such as difficulties applying impact tests to the tool tip or mass of the acceleration. Moreover, removing material and continuously changing spindle location can cause variations in the dynamic properties. Therefore, a passive absorber such as TMD or an inerter-based absorber is expected to be sufficiently robust against these changes. Therefore, a brief robustness analysis is now conducted to assess whether the proposed system is more susceptible to mistuning than a traditional vibration absorber.

The robustness of the inerter based absorber was evaluated for uncertainties in the dynamic features (K, f_n and ζ_m) in the main structural system. For this, Monte Carlo simulation was conducted for 250 runs assuming a normal distribution for all three parameters. The mean and standard deviation (σ) values are given in Table 4 for each parameter.

The robustness analysis was conducted for the TMD, the ideal IDVA and the practical IDVA using the milling parameters used in the experiments. The results are demonstrated in Fig. 10. Both the ideal and practical IDVAs presented almost the same robustness. The IDVA showed overall higher robustness, especially in the range of 2000-3000 rpm, around the flat side of the first lobe. This region is where the stability was maximised in the optimisation. The TMD indicated higher robustness near the resonance region, around 1700-2000 rpm. This region is where the lobbing effects are seen. It is worth reminding that all control devices were tuned for absolute stability and thus, there is no benefit in using control devices with these parameters for the lobbing effect. With the results in the previous and this section, the inerter-based absorber provided higher absolute stability and higher robustness.

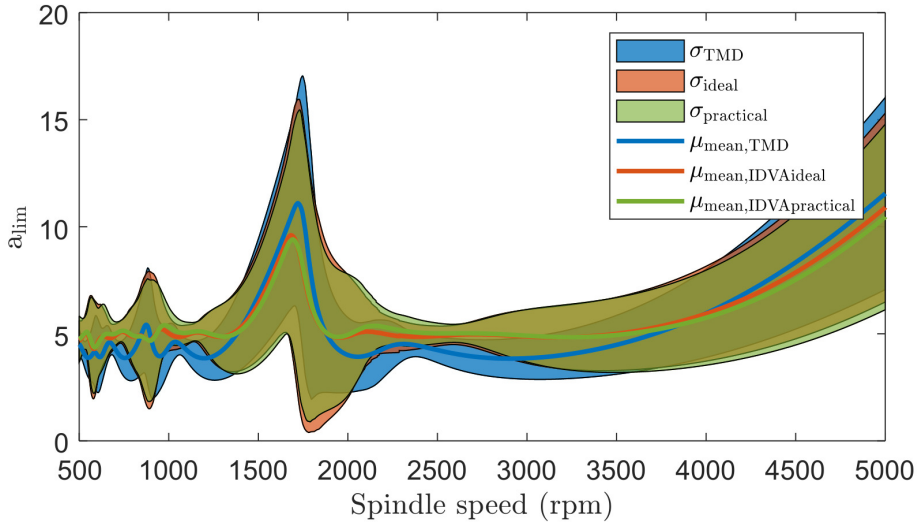

Fig. 10: Robustness of the TMD, the ideal IDVA, and the practical IDVA obtained by Monte Carlo simulation. Each curve shows the mean value and each filled region indicates 95% confidence interval.

A final aspect of this robustness problem relates to the sign of the directional factor, which is a consequence of the cutting conditions (feed direction and radial immersion). For the simplified scenario considered in this study, the directional factor is just a constant in Eq. 1. Therefore, in the context of this study, it has no effect but acts as a gain, as long as its sign remains the same. With the milling parameters used in the manuscript, the directional factor has a positive sign, so the real part of the FRF is maximised for equal troughs. When the sign becomes negative, the real part is optimised for equal peaks. The optimal design parameters for these two cases are completely different, as is the case for traditional vibration absorbers. This means that when the sign of the direction factor changes, the control device becomes completely detuned, whether it is a vibration absorber or an IDVA. This practical aspect needs to be carefully considered when designing such devices.

7 CONCLUSION

Passive control devices such as TMDs have commonly been used for chatter suppression, which is a stability problem as distinct from forced vibrations. Inerter-based absorbers can be used to give better performances than classical passive control approaches by improving the vibration mitigation effect. This paper presented the implementation of an inerter-based vibration absorber in milling focusing on chatter suppression for the first time. The practical IDVA configuration based on an idealised TID was numerically evaluated to show the potential stability improvement. Numerical optimisation was utilised to obtain the optimal design parameters. The absolute stability improvement compared to the TMD was experimentally validated using milling trials. This paper presents the first experimental implementation of an inerter for chatter stability problems. There was excellent agreement with the theoretical performance predictions, indicating a 16% improvement in stability compared to an idealised classical TMD, and over a four-fold im-

provement compared to an uncontrolled system with no TMD. Finally, it was shown that the IDVA is more robust than the TMD for the absolute stability for the case studied in this paper.

Attachment of the prototype without the need for a grounded connection provided a versatile solution allowing its use in a similar way to a classical TMD. The proposed design of the IDVA in this paper was mainly considered for the proof of the concept. It is possible to use the IDVA for smaller flexible workpieces with a smaller scale prototype, which could be considered for the future prototypes. Alternative damping solution such as eddy currents or elastomers can adapted to make the device more favourable for industrial applications. Furthermore, there is the potential that inerters can be employed for not only flexible workpieces, but also other modes of the machine tool system. For example, use of the inerter for chatter caused by the machine structure, tool or spindle could be considered in future work. In addition, optimisation strategies could focus on reshaping the stability lobes themselves, such as increasing the maximum stability and manipulating the lobbing effect, rather than the absolute stability limit that was considered in the present study.

ACKNOWLEDGEMENTS

HD would like to acknowledge the support from the Turkish Ministry of National Education by providing the scholarship.

REFERENCES

[1] Dogan, H., Sims, N. D., and Wagg, D. J., 2022, "Design, testing and analysis of a pivoted-bar inerter device used as a vibration absorber," *Mechanical Systems and Signal Processing,* **171**(February), p. 108893.

[2] Hahn, R. S., 1951, "Design of Lanchester damper for elminiation of metal-cutting chatter," *Journal of Engineering for Industry,* **73**(3), pp. 331–335.

[3] Tobias, S. A., 1965, *Machine tool vibration* Blackie and Sons Ltd.

[4] Rivin, E. I., and Kang, H., 1992, "Enhancement of dynamic stability of cantilever tooling structures," pp. 539–561.

[5] Tarng, Y. S., Kao, J. Y., and Lee, E. C., 2000, "Chatter suppression in turning operations with a tuned vibration absorber," *Journal of Materials Processing Technology,* **105**, pp. 55–60.

[6] Den Hartog, J. P., 1956, *Mechanical vibrations* McGraw-Hill, New York.

[7] Tobias, S. A., and Fishwick, W., 1958, "Theory of regenerative machine tool chatter," *The Engineer*.

[8] Tlusty, J., and Polacek, M., 1963, "The stability of the machine tool against self-excited vibration in machining," *International Research in Production Engineering,* **1**(2), pp. 465 – 474.

[9] Sims, N. D., 2007, "Vibration absorbers for chatter suppression: A new analytical tuning methodology," *Journal of Sound and Vibration,* **301**, pp. 592–607.

[10] Miguélez, M. H., Rubio, L., Loya, J. A., and Fernández-Sáez, J., 2010, "Improvement of chatter stability in boring operations with passive vibration absorbers," *International Journal of Mechanical Sciences,* **52**(10), pp. 1376–1384.

[11] Rubio, L., Loya, J. A., Miguélez, M. H., and Fernández-Sáez, J., 2013, "Optimization of passive vibration absorbers to reduce chatter in boring," *Mechanical Systems and Signal Processing,* **41**(1-2), pp. 691–704.

[12] Rashid, A., and Nicolescu, C. M., 2008, "Design and implementation of tuned viscoelastic

dampers for vibration control in milling," *International Journal of Machine Tools and Manufacture,* **48**(9), pp. 1036–1053.

[13] Munoa, J., Iglesias, A., Olarra, A., Dombovari, Z., Zatarain, M., and Stepan, G., 2016, "Design of self-tuneable mass damper for modular fixturing systems," *CIRP Annals - Manufacturing Technology,* **65**(1), pp. 389–392.

[14] Yang, Y., Xie, R., and Liu, Q., 2017, "Design of a passive damper with tunable stiffness and its application in thin-walled part milling," *International Journal of Advanced Manufacturing Technology,* **89**, pp. 2713–2720.

[15] Yuan, H., Wan, M., Yang, Y., and Zhang, W. H., 2019, "A tunable passive damper for suppressing chatters in thin-wall milling by considering the varying modal parameters of the workpiece," *International Journal of Advanced Manufacturing Technology,* **104**(9-12), pp. 4605–4616.

[16] Yuan, H., Wan, M., and Yang, Y., 2019, "Design of a tunable mass damper for mitigating vibrations in milling of cylindrical parts," *Chinese Journal of Aeronautics,* **32**(3).

[17] Yadav, A., Talaviya, D., Bansal, A., and Law, M., 2020, "Design of chatter-resistant damped boring bars using a receptance coupling approach," *Journal of Manufacturing and Materials Processing,* **4**(2).

[18] Ma, W., Yu, J., Yang, Y., and Wang, Y., 2020, "Optimization and tuning of passive tuned mass damper embedded in milling tool for chatter mitigation," *Journal of Manufacturing and Materials Processing,* **5**(1), p. 2.

[19] Yang, Y., Muñoa, J., and Altintas, Y., 2010, "Optimization of multiple tuned mass dampers to suppress machine tool chatter," *International Journal of Machine Tools and Manufacture,* **50**(9), pp. 834–842.

[20] Nakano, Y., Takahara, H., and Kondo, E., 2013, "Countermeasure against chatter in end milling operations using multiple dynamic absorbers," *Journal of Sound and Vibration,* **332**(6), pp. 1626–1638.

[21] Wang, M., Zan, T., Yang, Y., and Fei, R., 2010, "Design and implementation of nonlinear TMD for chatter suppression: An application in turning processes," *International Journal of Machine Tools and Manufacture,* **50**(5), pp. 474–479.

[22] Wang, M., 2011, "Feasibility study of nonlinear tuned mass damper for machining chatter suppression," *Journal of Sound and Vibration,* **330**(9), pp. 1917–1930.

[23] Habib, G., Kerschen, G., and Stepan, G., 2017, "Chatter mitigation using the nonlinear tuned vibration absorber," *International Journal of Non-Linear Mechanics,* **91**, pp. 103–112.

[24] Yang, Y., Dai, W., and Liu, Q., 2014, "Design and implementation of two-degree-of-freedom tuned mass damper in milling vibration mitigation," *Journal of Sound and Vibration,* **335**, pp. 78–88.

[25] Yang, Y., Dai, W., and Liu, Q., 2017, "Design and machining application of a two-DOF magnetic tuned mass damper," *International Journal of Advanced Manufacturing Technology,* **89**(5-8), pp. 1635–1643.

[26] Smith, M. C., 2002, "Synthesis of mechanical networks: The inerter," *IEEE Transactions on Automatic Control,* **47**(10), pp. 1648–1662.

[27] Papageorgiou, C., Houghton, N. E., and Smith, M. C., 2009, "Experimental testing and analysis of inerter devices," *Journal of Dynamic Systems, Measurement and Control, Transactions of the ASME,* **131**(1), pp. 1–11.

[28] Chen, M. Z., Papageorgiou, C., Scheibe, F., Wang, F. C., and Smith, M., 2009, "The missing mechanical circuit element," *IEEE Circuits and Systems Magazine,* **9**(1), pp. 10–26.

[29] Wang, F. C., and Su, W. J., 2008, "Impact of inerter nonlinearities on vehicle suspension control," *Vehicle System Dynamics,* **46**(7), pp. 575–595.
[30] Swift, S. J., Smith, M. C., Glover, A. R., Papageorgiou, C., Gartner, B., and Houghton, N. E., 2013, "Design and modelling of a fluid inerter," *International Journal of Control,* **86**(11), pp. 2035–2051.
[31] De Domenico, D., Deastra, P., Ricciardi, G., Sims, N. D., and Wagg, D. J., 2018, "Novel fluid inerter based tuned mass dampers for optimised structural control of base-isolated buildings," *Journal of the Franklin Institute,* **356**(14).
[32] John, E. D. A., and Wagg, D. J., 2019, "Design and testing of a frictionless mechanical inerter device using living-hinges," *Journal of the Franklin Institute,* **356**(14), pp. 7650–7668.
[33] Smith, M. C., 2020, "The inerter: A retrospective," *Annual Review of Control, Robotics, and Autonomous Systems,* **3**(1), pp. 361–391.
[34] Wagg, D. J., 2021, "A review of the mechanical inerter : historical context , physical realisations and nonlinear applications," *Nonlinear Dynamics*.
[35] Smith, M. C., and Wang, F. C., 2004, "Performance benefits in passive vehicle suspensions employing inerters," *Vehicle System Dynamics,* **42**(4), pp. 235–257.
[36] Jiang, J. Z., Maramoros-Sanchez, A. Z., Goodall, R. M., and Smith, M. C., 2012, "Passive suspension incorporating inerters for railway vehicles," *Vehicle System Dynamics,* **50**, pp. 263–276.
[37] Li, Y., Jiang, J. Z., Neild, S. A., and Wang, H., 2017, "Optimal inerter-based shock–strut configurations for landing-gear touchdown performance," *Journal of Aircraft,* **54**(5), pp. 1901–1909.
[38] Li, Y., Jiang, J. Z., and Neild, S., 2017, "Inerter-based configurations for main-landing-gear shimmy suppression," *Journal of Aircraft,* **54**(2), pp. 684–693.
[39] Lazar, I. F., Neild, S. A., and Wagg, D. J., 2014, "Using an inerter-based device for structural vibration suppression," *Earthquake Engineering and Structural Dynamics,* **43**(8), pp. 1129–1147.
[40] Giaralis, A., and Taflanidis, A. A., 2018, "Optimal tuned mass-damper-inerter (TMDI) design for seismically excited MDOF structures with model uncertainties based on reliability criteria," *Structural Control and Health Monitoring,* **25**(2), pp. 1–22.
[41] Shi, X., and Zhu, S., 2018, "Dynamic characteristics of stay cables with inerter dampers," *Journal of Sound and Vibration,* **423**, jun, pp. 287–305.
[42] Hu, Y., Wang, J., Chen, M. Z. Q., Li, Z., and Sun, Y., 2018, "Load mitigation for a barge-type floating off shore wind turbine via inerter-based passive structural control," *Engineering Structures,* **177**(15), pp. 198–209.
[43] Marian, L., and Giaralis, A., 2014, "Optimal design of a novel tuned mass-damper-inerter (TMDI) passive vibration control configuration for stochastically support-excited structural systems," *Probabilistic Engineering Mechanics,* **38**, pp. 156–164.
[44] Ikago, K., Saito, K., and Inoue, N., 2012, "Seismic control of single-degree-of-freedom structure using tuned viscous mass damper," *Earthquake Engineering and Structural Dynamics,* **41**, pp. 453–474.
[45] Hu, Y., and Chen, M. Z. Q., 2015, "Performance evaluation for inerter-based dynamic vibration absorbers," *International Journal of Mechanical Sciences,* **99**, pp. 297–307.
[46] Hu, Y., Chen, M. Z. Q., Shu, Z., and Huang, L., 2015, "Analysis and optimisation for inerter-based isolators via fixed-point theory and algebraic solution," *Journal of Sound and Vibration,* **346**, pp. 17–36.

[47] Barredo, E., Blanco, A., Colín, J., Penagos, V. M., Abúndez, A., Vela, L. G., Meza, V., Cruz, R. H., and Mayén, J., 2018, "Closed-form solutions for the optimal design of inerter-based dynamic vibration absorbers," *International Journal of Mechanical Sciences,* **144**, pp. 41–53.

[48] Dogan, H., Sims, N. D., and Wagg, D. J., 2019, "Investigation of the inerter-based dynamic vibration absorber for machining chatter suppression," *Journal of Physics: Conference Series,* **1264**.

[49] Wang, F. C., Lee, C. H., and Zheng, R. Q., 2019, "Benefits of the inerter in vibration suppression of a milling machine," *Journal of the Franklin Institute,* **356**(14), pp. 7689–7703.

[50] Budak, E., and Altintas, Y., 1998, "Analytical prediction of chatter stability in milling — Part I : General formulation," *Journal Of Dynamic Systems Measurement And Control,* **120**, pp. 22–30.

[51] Budak, E., and Altintas, Y., 1998, "Analytical prediction of chatter stability in milling - Part II: Application of the general formulation to common milling systems," *Journal Of Dynamic Systems Measurement And Control,* **120**, pp. 31–36.

[52] Davies, M. A., Pratt, J. R., Dutterer, B., and Burns, T. J., 2002, "Stability prediction for low radial immersion milling," *Journal of Manufacturing Science and Engineering,* **124**, pp. 217–225.

[53] Qin, A. K., Huang, V. L., and Suganthan, P. N., 2009, "Self-adaptive differential evolution algorithm for numerical optimization," *IEEE Communications Magazine,* **13**(2), pp. 398–417.

[54] Worden, K., and Manson, G., 2012, "On the identification of hysteretic systems. Part I: Fitness landscapes and evolutionary identification," *Mechanical Systems and Signal Processing,* **29**, pp. 201–212.

[55] Almagirby, A., Rongong, J. A., and Carré, M. J., 2018, "The development of a new artificial model of a finger for assessing transmitted vibrations," *Journal of the Mechanical Behavior of Biomedical Materials,* **78**, pp. 20–27.

[56] Deastra, P., Wagg, D. J., Sims, N. D., and Mills, R. S., 2022, "Experimental shake table validation of damping behaviour in inerter-based dampers," *Bulletin of Earthquake Engineering*(2002).

[57] Sims, N., 2005, "The self-excitation damping ratio: A chatter criterion for time-domain milling simulation," *Journal of Manufacturing Science and Engineering,* **127**, pp. 433–445.

[58] Schmitz, T. L., 2003, "Chatter recognition by a statistical evaluation of the synchronously sampled audio signal," *Journal of Sound and Vibration,* **262**, pp. 721–730.

[59] Insperger, T., Mann, B. P., Surmann, T., and Stépán, G., 2008, "On the chatter frequencies of milling processes with runout," *International Journal of Machine Tools and Manufacture,* **48**(10), pp. 1081–1089.

APPENDIX A: FULL EXPRESSIONS FOR THE DIMENSIONLESS FRF

Full expressions for R_n, R_d, I_n and I_d for the idealised and practical IDVAs in Eq. 6 are given as following:

$$
\begin{aligned}
R_{n,idealised} &= -\delta\Big(-\Omega^4+\gamma^2(1+(\delta+1)\alpha^2)\Omega^2-\alpha^2\gamma^4\Big)\\
I_{n,idealised} &= -2\zeta_a\gamma\big((\delta+1)\Omega^2-\gamma^2\big)\Omega\\
R_{d,idealised} &= -\delta\Omega^6+\Big(\alpha^2\gamma^2(\mu+1)\delta^2+\big(1+(\alpha^2+\mu+1)\gamma^2+4\gamma\zeta_a\zeta_m\big)\delta+4\gamma\zeta_a\zeta_m\Big)\Omega^4-\gamma^2\Big(\alpha^2\delta^2+(\alpha^2\gamma^2(\mu+1)+\alpha^2+1)\delta+4\gamma\zeta_a\zeta_m\Big)\Omega^2+\delta\gamma^4\alpha^2\\
I_{d,idealiased} &= 2\Omega\Big(\Big(\zeta_a\big(1+(\mu+1)\delta\big)\gamma+\zeta_m\delta\Big)\Omega^4-\gamma\Big(\zeta_a(\mu+1)\gamma^2+\delta\zeta_m(\delta\alpha^2+\alpha^2+1)\gamma+\zeta_a(\delta+1)\Big)\Omega^2+\gamma^3(\delta\alpha^2\gamma\zeta_m+\zeta_a)\Big)
\end{aligned}
$$

$$
\begin{aligned}
R_{n,practical} &= (\beta+\delta)\,\Omega^4+\left((\alpha^2(\eta^2-1)\delta^2+(-1+(\beta\eta^2+\ eta a^2-\beta-1)\alpha^2)\delta-\beta)\gamma^2-\beta\kappa^2\right)\Omega^2-\left(\delta\,(\eta-1)\,(\eta+1)\left(\beta\,\kappa^2+\gamma^2\right)\alpha^2-\beta\,\kappa^2\right)\gamma^2\\
I_{n,practical} &= (\beta+\delta)\,\eta\Omega^4+\left(\left(2\alpha^2\delta^2+\left(1+2\,(\beta+1)\,\alpha^2\right)\delta+\beta\right)\gamma^2+\beta\kappa^2\right)\eta\Omega^2+2\gamma^2\left(\alpha^2\delta\gamma^2+\kappa^2\left(\alpha^2\delta+\frac{1}{2}\right)\beta\right)\eta\\
R_{d,practical} &= -\left(\beta\delta\mu+\beta+\delta\right)\Omega^6-2\eta\zeta_m\left(\beta+\delta\right)\Omega^5\\
&\quad-\left(\alpha^2\gamma^2\left(\eta-1\right)\left(\eta+1\right)\left(\beta\mu+\mu+1\right)\delta^2+\left(\left(\left(\eta^2-1\right)\alpha^2-\mu\right)\beta+\left(\eta^2-1\right)\alpha^2-\mu-1\right)\gamma^2-\mu\beta\,\kappa^2-1\right)\delta-\beta\left(\left(\mu+1\right)\gamma^2+\mu\beta\kappa^2+\kappa^2+1\right)\right)\Omega^4\\
&\quad+4\left(\left(\alpha^2\delta^2+\left(\frac{1}{2}+\left(\beta+1\right)\alpha^2\right)\delta+\frac{\beta}{2}\right)\gamma^2+\frac{\kappa^2\beta}{2}\right)\zeta_m\eta\Omega^3\\
&\quad+\left(\alpha^2\delta\left(\eta-1\right)\left(\eta+1\right)\left(\beta\mu+\mu+1\right)\gamma^4+\left(\alpha^2\left(\eta-1\right)\left(\eta+1\right)\left(\mu\beta\kappa^2+1\right)\delta^2+\left(\left(\eta+1\right)\left(\eta-1\right)\left(1+\kappa^2\mu\beta^2+\left(1+\left(\mu+1\right)\kappa^2\right)\beta\right)\alpha^2-\mu\beta\kappa^2-1\right)\delta-\left(\mu\beta\kappa^2+1+\left(\mu+1\right)\kappa^2\right)\beta\right)\gamma^2-\kappa^4\mu\beta^2-\kappa^2\beta\right)\Omega^2\\
&\quad-4\left(\delta\left(\kappa^2\beta+\gamma^2\right)\alpha^2+\frac{\kappa^2\beta}{2}\right)\zeta_m\eta\gamma^2\Omega-\left(\delta\left(\eta-1\right)\left(\eta+1\right)\left(\kappa^2\beta+\gamma^2\right)\alpha^2-\kappa^2\beta\right)\gamma^2\left(\mu\beta\kappa^2+1\right)\\
I_{d,practical} &= -\eta\left(\beta\delta\mu+\beta+\delta\right)\Omega^6+2\zeta_m\left(\beta+\delta\right)\Omega^5+\left(2\alpha^2\gamma^2\left(\beta\mu+\mu+1\right)\delta^2+\left(\left(2\alpha^2+\mu\right)\beta+2\alpha^2+\mu+1\right)\gamma^2+\mu\beta\,\kappa^2+1\right)\delta+\beta\left(\left(\mu+1\right)\gamma^2+\mu\beta\,\kappa^2+\kappa^2+1\right)\right)\eta\Omega^4\\
&\quad+2\left(\left(\alpha^2\left(\eta^2-1\right)\delta^2+\left(-1+\left(\beta\,\eta^2+\eta^2-\beta-1\right)\alpha^2\right)\delta-\beta\right)\gamma^2-\beta\,\kappa^2\right)\zeta_m\Omega^3-\eta\left(\left(\left(1+\left(\mu+1\right)\kappa^2\right)\beta+2\alpha^2\delta^2+2\alpha^2\delta+\delta\right)\gamma^2+\beta\,\kappa^2\right)\Omega^2-2\left(\delta\left(\eta-1\right)\left(\eta+1\right)\left(\beta\,\kappa^2+\gamma^2\right)\alpha^2-\beta\,\kappa^2\right)\Omega\\
&\quad\zeta_m\gamma^2+2\gamma^2\eta\left(\alpha^2\delta\,\gamma^2+\beta\,\kappa^2\left(\alpha^2\delta+\frac{1}{2}\right)\right)\left(\mu\beta\,\kappa^2+1\right)
\end{aligned}
$$